Available online at www.sciencedirect.com
ScienceDirect
Journal of Catalysis 256 (2008) 37–44
JOURNAL OF CATALYSIS
www.elsevier.com/locate/jcat

Deactivation and regeneration behaviors of copper spinel–alumina composite catalysts in steam reforming of dimethyl ether

Kajornsak Faungnawakij [a,b], Tetsuya Fukunaga [c], Ryuji Kikuchi [b], Koichi Eguchi [b,*]

[a] *Japan Science and Technology Agency (JST), JST Innovation Plaza Kyoto, 1-30 Goryo-Ohara, Nishikyo-ku, Kyoto 615-8245, Japan*
[b] *Department of Energy and Hydrocarbon Chemistry, Graduate School of Engineering, Kyoto University, Nishikyo-ku, Kyoto 615-8510, Japan*
[c] *Central Research Laboratories, Idemitsu Kosan Co., Ltd., 1280 Kami-izumi, Sodegaura, Chiba 299-0293, Japan*

Received 19 December 2007; revised 21 February 2008; accepted 25 February 2008

Abstract

The durability of composite catalysts of $CuFe_2O_4$ and γ-Al_2O_3 was investigated during steam reforming (SR) of dimethyl ether (DME). Partial degradation of the composites proceeded due to the concomitant effect of copper sintering and carbon formation. The catalyst degraded after SR for 1100 h was regenerated by calcination in air in the temperature range of 500–700 °C; redispersion of copper via spinel formation and simultaneous carbon burning were achieved. The apparent activation energy for DME SR over the catalyst was estimated to be in the range of 150–160 kJ mol^{-1} and remained almost stable during the DME SR reaction test for 1100 h. Degradation of the catalyst was found to follow first-order kinetics with a deactivation rate constant of 0.95×10^{-3} h^{-1}.

Keywords: Deactivation; Regeneration; Cu spinel; Coking; Sintering; Steam reforming; Dimethyl ether

1. Introduction

Utilization of hydrogen is of interest in the field of new energy, especially fuel cells. Fuel cells are considered efficient and environmentally friendly power generators, because electrical energy can be generated directly from chemical energy without pollutant emission. Fuel cells have been investigated in both mobile and stationary applications [1]. Typically, an electrochemical reaction of a fuel at anode (generally H_2) and an oxidant at cathode (generally O_2) generates electricity through a fuel cell, with only water produced onsite as a single chemical product.

Efficient production of hydrogen from various fuels is considered one of the key factors for commercialization of fuel cells. Steam reforming (SR), partial oxidation (PO), and oxidative steam reforming (OSR) or autothermal reforming (ATR) are established H_2 generation reactions with differing characteristics. Endothermic SR is more attractive than the other methods because of its high H_2 yield and product qualities.

A number of fuels, including methane, liquefied petroleum gas (LPG), gasoline, ethanol (EtOH), methanol (MeOH), and dimethyl ether (DME), have been used as H_2 sources in the aforementioned reactions. Among these, DME SR is recognized as a promising process for H_2 production [2]. DME is a harmless oxygenated hydrocarbon that provides a high hydrogen-to-carbon ratio that has been used as a clean-burning fuel alternative to LPG and diesel. The well-developed infrastructure of LPG can readily be adapted for DME because of their similar physical properties. DME and MeOH are suitable for on-board reforming because they can be reformed catalytically at low temperatures (200–350 °C for MeOH [3–8] and 200–400 °C for DME [9–18]). DME is less toxic and thus is preferable to MeOH.

DME SR (Reaction (1)) comprises two moderately endothermic reactions in sequence: hydrolysis of DME to MeOH (Reaction (2)) and SR of the resultant MeOH to hydrogen and carbon dioxide (Reaction (3)):

* Corresponding author. Fax: +81 75 383 2520.
E-mail addresses: kajornsak_f@yahoo.com (K. Faungnawakij), eguchi@scl.kyoto-u.ac.jp (K. Eguchi).

0021-9517/$ – see front matter
doi:10.1016/j.jcat.2008.02.022

DME SR:

$$(CH_3)_2O\ (g) + 3H_2O\ (g) \rightarrow 6H_2\ (g) + 2CO_2\ (g), \quad \Delta H_r^0 = 135\ \mathrm{kJ\,mol^{-1}}, \tag{1}$$

DME hydrolysis:

$$(CH_3)_2O\ (g) + H_2O\ (g) \rightarrow 2CH_3OH\ (g), \quad \Delta H_r^0 = 37\ \mathrm{kJ\,mol^{-1}}, \tag{2}$$

MeOH SR:

$$CH_3OH\ (g) + H_2O\ (g) \rightarrow 3H_2\ (g) + CO_2\ (g), \quad \Delta H_r^0 = 49\ \mathrm{kJ\,mol^{-1}}. \tag{3}$$

Hydrolysis of DME occurs over acid catalysts (e.g., zeolite and alumina), whereas MeOH SR proceeds over Cu-, Pt-, and Pd-based catalysts. Consequently, composite catalysts of the acid catalysts and the metal-based catalysts are generally needed for DME SR. Copper-based catalysts are promising in terms of cost-effectiveness and activity. Various solid acids, such as zeolite and alumina, have been proposed as DME hydrolysis catalysts. Zeolites, such as Y, ZSM-5, and H-mordenite and WO_3/ZrO_2, have exhibited high hydrolysis activity due to their strong acid sites; however, severe degradation also has been observed [13,16,19]. Gamma-alumina has relatively weak acid sites and thus provides lower activity. Nevertheless, good durability is expected from the weak acidity, which provokes few side reactions. A high reaction temperature (above 300 °C) is required for effective hydrolysis of DME over γ-Al_2O_3. The high reaction temperature brings about severe sintering of Cu in the composite catalysts.

We have proposed Cu-based spinels mixed with γ-Al_2O_3 for DME SR and demonstrated that the composite catalysts exhibited excellent catalytic performance in DME SR compared with Cu/ZnO and Cu/ZnO/Al_2O_3 [18,19]. Moving to the next stage requires insight into the deactivation behavior of the composite catalysts in the high-temperature range for implementation and commercialization of H_2 production systems using DME SR. Regeneration of degraded composites of the Cu spinel and γ-Al_2O_3 are of interest for practical uses as well.

In the present work, the degradation behavior of the composites of $CuFe_2O_4$ and γ-Al_2O_3 in DME SR was studied over a reaction time of 1000 h. The regenerability of degraded catalysts after the long-term tests also was investigated. The fresh, degraded, and regenerated composites were characterized to clarify the origin of deactivation and regeneration.

2. Experimental

2.1. Catalyst preparation

Spinel $CuFe_2O_4$ was prepared by a sol–gel method from citrate complex. This method can effectively accommodate different cations in the complex, resulting in uniform mixing of the cations. An aqueous solution of copper and iron nitrates [$Cu(NO_3)_2{\cdot}3H_2O$ and $Fe(NO_3)_3{\cdot}9H_2O$] was stirred at 60 °C for 2 h, followed by addition of citric acid. Subsequently, the solution was kept at 60 °C for 1 h, and then heated up to 90 °C to evaporate water. The resultant precipitate was heated up to 140–200 °C until fine oxide powder was obtained. The powder was calcined in air at 900 °C for 10 h to form a $CuFe_2O_4$ spinel phase of high crystallinity [18]. Gamma-alumina (ALO8), provided by the Catalysis Society of Japan, was calcined in air at 700 °C for 0.5 h before mechanical mixing with the spinel. Composite catalysts of Cu spinel and γ-Al_2O_3 were prepared by mechanical milling in a mortar at a fixed weight ratio of 2:1. After mixing, the composite was heat-treated in air at 700 °C for 10 h and then pressed, crushed, and sieved to particle sizes of 0.85–1.7 mm.

2.2. Catalyst characterization

A nitrogen adsorption system (BEL Japan Bellsorp–miniπ) was used to measure the adsorption–desorption isotherm at a liquid nitrogen temperature of −196 °C. The Brunauer–Emmett–Teller (BET) and the Barrett–Joyner–Halenda (BJH) approaches were used to determine the surface area and pore size distribution of the samples, respectively. Temperature-programmed oxidation (TPO) was used to analyze the amount of carbon deposited on the catalyst surface.

A 50-mg catalyst sample was oxidized in 5% O_2/He at a flow rate of 30 ml min^{-1} (25 °C, 1 atm) in a heating process at a rate of 10 °C min^{-1}. The product gases were monitored by online mass spectrometry. Powder X-ray diffraction (XRD) patterns were obtained using a Rigaku RINT-2200 with a CuK_α radiation source ($\lambda = 0.15406$ nm), operated at 40 kV and 40 mA. The crystallite size was calculated by XRD line-broadening using Scherrer's equation. X-ray photoelectron spectroscopy (XPS) was performed using a Shimadzu ESCA-850 with a MgK_α radiation source. Raman spectra were measured using a JOBIN YVON T64000 equipped with a CCD detector and a 514-nm laser. Fourier transform infrared (FTIR) spectroscopy was carried out using a Jasco FT/IR-410.

2.3. Catalyst activity–durability evaluation

Catalytic activity was evaluated using a conventional flow reactor under atmospheric pressure. The reactor's configuration is shown schematically in Fig. 1. Thermocouples were inserted at a constant interval of 1 cm along the axial length of the reactor mounted vertically in the experimental unit. (Hereinafter, the local reaction temperature in the catalyst bed is referred to as the "catalyst temperature.") The reactor was set inside a conventional furnace, and the furnace setpoint temperature is set adjacent to the outer surface of the reactor. (Hereinafter, this setpoint temperature is called the "temperature.") The composite catalysts were evaluated without prereduction before the DME SR reaction, unless stated otherwise. A gas mixture of steam and DME at a fixed steam-to-carbon ratio (S/C) of 2.5 (at 25 °C; 1 atm) was supplied through mass flow controllers to a preheater at ca. 150 °C and then to the catalyst bed set at the reaction temperature.

Long-term reaction tests were carried out to investigate deactivation behavior in the following manner. The reaction tem-

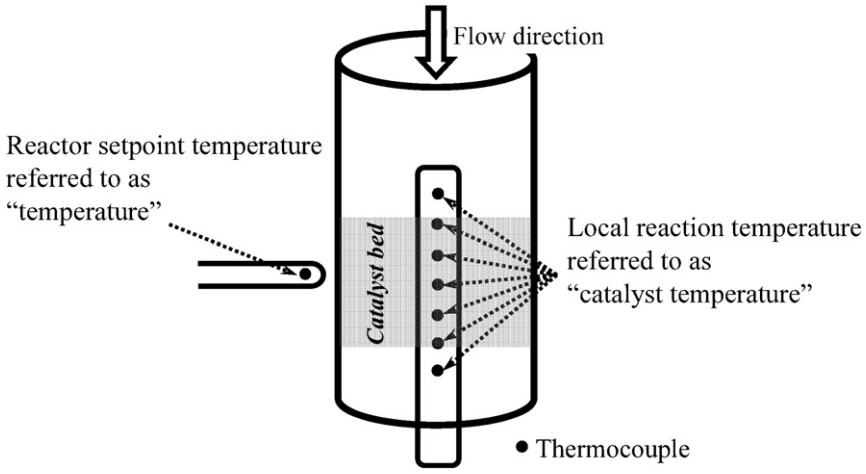

Fig. 1. Configuration of reactor and reaction temperature measurement points.

perature was raised from 255 to 380 °C at a heating rate of 2.5 °C min^{-1}, and gas analysis was performed from 255 °C at a constant temperature interval of 25 °C. Before the gas analysis, the reaction temperature was held for 1 h. After the temperature reached the final setpoint at 380 °C, it was kept constant for ca. 100 h; gas analysis was carried out periodically during this period. After the period of constant temperature at 380 °C, the reaction temperature was dropped to 255 °C, and the next measurement cycle was started. After the long-term reaction test was completed, all of the reacted catalysts were cooled to room temperature in N_2 flow and then exposed to air. Reformate gas was flowed through a steam-trapping condenser at ca. 3 °C before the gas analysis. Compositions of feed and effluent gas were analyzed by online gas chromatographs equipped with a flame ionization detector (Shimadzu GC-9A) and a thermal conductivity detector (Varian CP-4900). A Poraplot U column was used for separation of DME, MeOH, and CO_2, and a molecular sieve 5A column was used for separation of H_2, O_2, N_2, CH_4, and CO. DME conversion and selectivity to C_1 species are defined as

$$\text{DME conversion (\%)} = 100\left(\frac{\sum F_{C_1}}{\sum F_{C_1} + 2F_{\text{DME}}}\right) \quad (4)$$

and

$$\text{selectivity to } C_1\text{species} = 100\frac{F_{C_1}}{\sum F_{C_1}}, \quad (5)$$

where F_{DME} and F_{C_1} are the molar flow rates of DME and C_1-containing products (CH_4, CO, and CO_2) in the effluent gas, respectively.

3. Results and discussion

3.1. Deactivation behavior

Fig. 2 shows DME conversion as a function of reaction time during DME SR over the composite catalyst of $CuFe_2O_4$ and Al_2O_3 for 1100 h. DME conversion was measured stepwise during the temperature ramp from 255 to 380 °C at a constant interval of 25 °C for evaluation of degradation behavior. As the

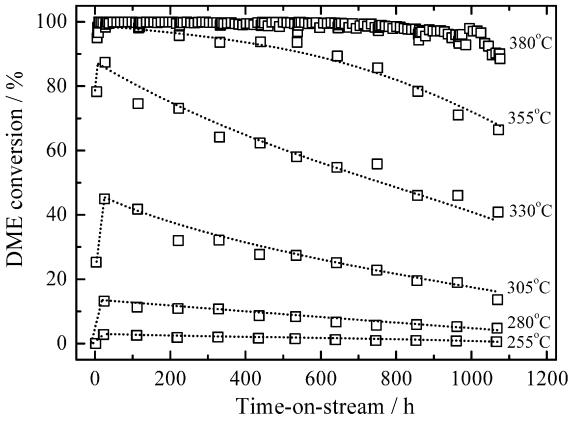

Fig. 2. Time-on-stream of DME conversion over composite of $CuFe_2O_4$ + Al_2O_3 in DME SR. Reaction conditions: S/C = 2.5; temperature sweep range from 255 to 380 °C; GHSV = 2000 h^{-1}; feed flow rate = 200 ml min^{-1}; catalyst amount = 6 cm^3.

reaction temperature was raised, DME conversion increased, and at 380 °C, complete conversion was attained for a reaction time of 800 h. The continuous decrease in DME conversion at low temperatures indicated that degradation of the composite catalyst proceeded gradually. The increased activity observed at a reaction time of 20–25 h was likely due to the formation of metallic Cu by *in situ* reduction of spinel under the working conditions; H_2 and CO were produced from the reforming reaction. Such activation during reaction was not observed over the prereduced catalyst.

Fig. 3 shows the product concentrations from the DME SR test (illustrated in Fig. 2). Here the representative data were obtained at a reaction temperature of 380 °C. Hydrogen-rich reformate was produced with high concentration (>70%). Concentrations of CO_2 and CO were ca. 23–24% and 2–4%, respectively, whereas that of CH_4 was <0.1%. No other products or intermediates were observed. A gradual decline in H_2 concentration was observed with increasing reaction time, whereas concentrations of CO_2 and CO remained unchanged. A hydrogen production rate of 50–60 mol kg$_{\text{cat}}^{-1}$ h^{-1} was obtained. All product species closely approached the equilibrium concen-

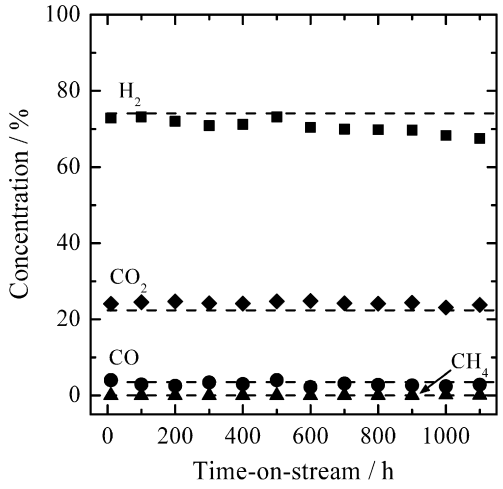

Fig. 3. Product concentration for DME SR at 380 °C over composite of $CuFe_2O_4$ and Al_2O_3 as a function of reaction time. Dashed lines represent the equilibrium concentrations.

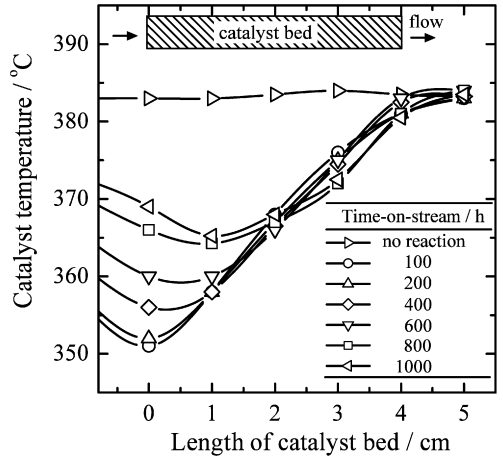

Fig. 4. Variation of local catalyst temperature along the catalyst bed with time-on-stream during DME SR test in Fig. 2. The deviation from the plot for no reaction indicates the temperature was lowered by the endothermic reaction.

tration calculated using Gibbs free energy minimization with a constraint condition of no methane or solid carbon species. Consequently, we can state that the composite catalyst developed in this study exhibited fairly good durability as well as activity in DME SR at high temperatures.

Although the reaction temperature remained constant at the outer surface of the reactor, the local catalyst temperatures were actually lower than the reactor temperature, due to the endothermic nature of DME SR reaction. Fig. 4 depicts axial profiles of catalyst temperature measured locally along the axis of the reactor during DME SR at a reaction temperature of 380 °C. Under N_2 flow, the catalyst temperature at the measurement points remained essentially constant along the bed at 383–384 °C. When the DME–steam mixture was fed to the bed, the catalyst temperature drastically dropped to ca. 365 °C at the inlet of the catalyst bed, and increased along the flow direction, up to ca. 383–385 °C at the end. The steep temperature profile reflects a high initial activity of the catalyst. Then, with increased reaction time, the steep decrease in the catalyst temperature at the inlet became smaller and the temperature profile became flattened, indicating expansion of the reaction zone along the flow direction. This temperature profile change suggests that partial degradation of the composite catalyst proceeded in the inlet zone, and eventually DME SR progressed in the entire catalyst bed.

3.2. Regeneration of degraded composite

The degraded composite catalyst after the long-term reaction test shown in Fig. 2 was regenerated by calcining in air at 375, 500, and 700 °C for 10 h. Temperature profiles of catalytic activity for DME SR over fresh, degraded, and regenerated catalysts are shown in Fig. 5a. Stability of the catalysts during DME SR at 370 and 380 °C is illustrated in Fig. 5b. All catalysts were prereduced at 250 °C in 10% H_2/N_2 for 3 h before testing. Note that reduction at 200–350 °C was not effective in regenerating the degraded composite. The degraded composite was partially regenerated by calcining in air at 375 °C, and the activity was fully recovered after heating at 500 and 700 °C. As shown in Fig. 5b, conversion of DME reached 100% at 380 °C over all of the catalysts except one that was regenerated at 375 °C.

XRD patterns of fresh, degraded, and regenerated composite catalysts are shown in Fig. 6. The fresh composite comprised Cu-based spinels, Fe_2O_3, and γ-Al_2O_3, whereas the degraded composite was transformed into three crystalline phases of metallic Cu, Fe_3O_4, and γ-Al_2O_3. Cu-based spinels were reduced *in situ* to metallic Cu and Fe_3O_4 under the working condition in H_2-containing reformate. After regeneration at 375 °C, crystalline phases assignable to Cu spinels, Fe_2O_3, CuO, and Al_2O_3 appeared in the XRD pattern; that is, partial reformation of Cu spinel proceeded. The formation of Cu spinels was evident at an increased regeneration temperature up to 500 °C and higher. The XRD pattern of the composite regenerated at 700 °C was almost identical to that of the fresh sample, which coincided with the recovery of reforming activity.

Based on the XRD analyses, the regeneration mechanism of $CuFe_2O_4$ spinel can be described through its reversible reduction process as follows: First, metallic Cu and Fe_3O_4 are oxidized to CuO and Fe_2O_3, respectively, and then Cu species incorporates with Fe_2O_3 to form spinel. The identical temperature-programmed reduction profiles of the fresh and regenerated spinel-based catalysts also confirm the spinel regeneration (results are not shown). Kameoka et al. [20] reported the formation of copper iron spinel structure through calcination of metallic copper and metallic iron, formed by reduction of $CuFe_2O_4$ with H_2 at 600 °C, at 800 °C in air.

Table 1 reports the Cu crystallite sizes in the spent catalysts and the BET surface areas of the fresh, regenerated, and spent catalysts. The spent composite catalysts were obtained after the reaction tests shown in Fig. 5. Based on an analysis of the XRD findings, all of the spent catalysts consisted of identical phases irrespective of the regeneration temperature. Despite the identical phases after the reaction test, the copper crystallite size was considerably larger in the spent composite calcined at

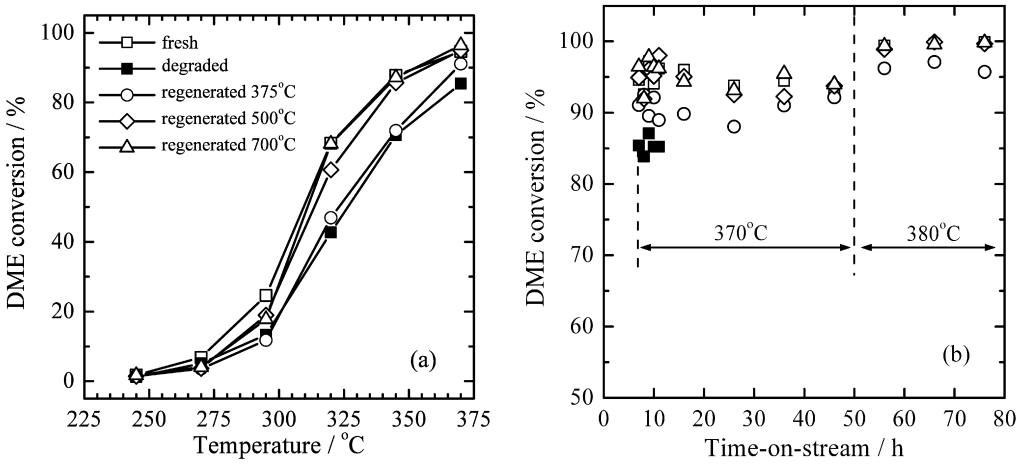

Fig. 5. (a) Temperature dependence of activities of fresh, degraded, and regenerated catalyst composed of $CuFe_2O_4$ and Al_2O_3, for DME SR and (b) conversion with time-on-stream at 370 and 380 °C. The degraded catalyst was obtained after the experiment in Fig. 2. All catalysts were prereduced at 250 °C for 3 h in H_2/N_2 prior to the reaction test. Reaction conditions: S/C = 2.5; GHSV = 2000 h^{-1}; catalyst amount = 2 cm^3.

Table 1
BET surface area and size of metallic copper in composites of $CuFe_2O_4$ and Al_2O_3

Catalysts	BET surface area ($m^2\ g^{-1}$)	Size of Cu[a] (nm)
(a) Fresh	34.2	–
(b) Regenerated at 375 °C[b]	34.9	–
(c) Regenerated at 500 °C[b]	36.4	–
(d) Regenerated at 700 °C[b]	27.3	–
(e) Spent (a)[c]	35.0	23.5
(f) Spent (b)[c]	35.4	36.0
(g) Spent (c)[c]	34.6	28.7
(h) Spent (d)[c]	26.8	22.1

[a] Calculated by XRD-line broadening technique using Scherrer's equation.
[b] Catalyst used for DME SR was regenerated by heating in air at respective temperatures for 10 h.
[c] Fresh and regenerated catalysts (a–d) were used for DME SR at the reaction conditions in Fig. 5.

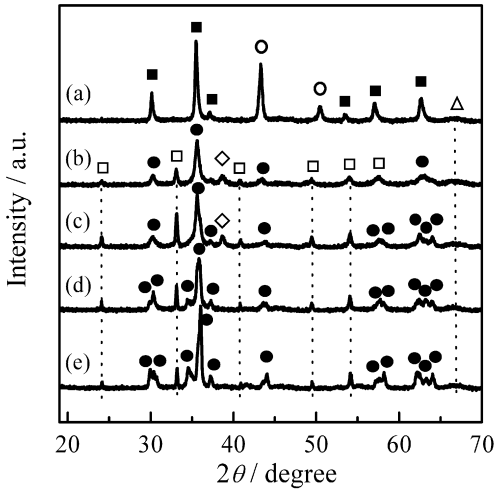

Fig. 6. XRD patterns of composites of $CuFe_2O_4$ and Al_2O_3 before and after reaction test and regeneration. (a) Degraded catalyst after the reaction in Fig. 2; (b) regenerated (a) in air at 375 °C; (c) regenerated (a) in air at 500 °C; (d) regenerated (a) in air at 700 °C; (e) fresh catalyst. (●) Cu-based spinels, (○) Cu, (◇) CuO, (■) Fe_3O_4, (□) Fe_2O_3, (△) Al_2O_3.

375 °C than in the composites regenerated at 500 and 700 °C. Regeneration at high temperatures (500 and 700 °C) resulted in reformation of the Cu spinel, which was subsequently reduced in situ under the working conditions, leading to redispersion of Cu species and recovery of the catalytic activity. On the other hand, calcination of the degraded catalyst at 375 °C was insufficient for complete reformation of the spinel, giving rise to sintering of Cu species, as indicated by the larger Cu crystallite sizes reported in Table 1. Compared with the $Cu/ZnO/Al_2O_3$ and Cu/ZnO catalysts, the Cu spinels were hardly sintered in the calcination process. The high sintering resistance of the $CuFe_2O_4$ spinel can be ascribed to the high dispersion of copper in the matrix of iron oxides and their strong interaction, accompanied by spinel formation. But recovery of fine copper species was incomplete at a low regeneration temperature of 375 °C, because spinel regeneration was insufficient due to the low heat treatment temperature, and sintering of Cu proceeded partially at a heat treatment temperature of 375 °C. The composite catalysts regenerated at 375 and 500 °C retained almost the same amount of surface area as the fresh one (ca. 34–36 $m^2\ g^{-1}$). The surface area did not change significantly after the long-term reaction test of 1100 h. The BET surface area decreased to ca. 27 $m^2\ g^{-1}$ after regeneration at 700 °C, which can be ascribed to the crystal growth and shrinkage of alumina grains. But, the smaller surface area did not affect the reforming activity, as shown in Fig. 5. The adsorption–desorption isotherm and the BJH pore size analysis confirmed a decrease in the pore volume of alumina. It is noteworthy that Cu spinel is nonporous, with as extremely low surface area of ca. 0.5–1 $m^2\ g^{-1}$.

3.3. Carbon deposition and copper sintering

Deactivation in the SR process is commonly attributed to sintering, carbon deposition (coking), poisoning, and a change in oxidation state [21–24]. A change in the oxidation state of copper usually results in a rapid decline in activity. A high oxidation state corresponded to low activity at the very initial stage of DME SR test. A high space velocity was intentionally used

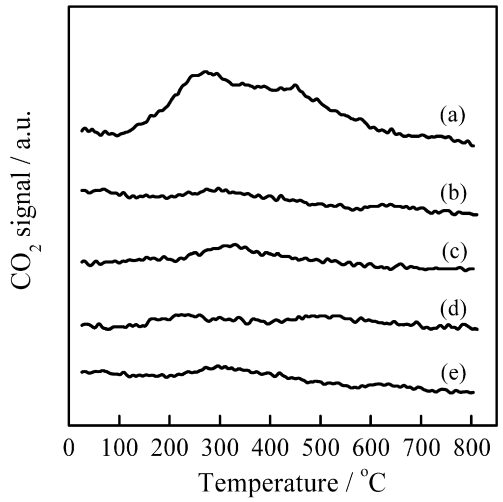

Fig. 7. Desorption curve of CO_2 during TPO of composite catalysts of $CuFe_2O_4$ and Al_2O_3. (a) Degraded catalyst after reaction in Fig. 2; (b) regenerated (a) in air at 375 °C; (c) regenerated (a) in air at 500 °C; (d) regenerated (a) in air at 700 °C; (e) fresh catalyst. TPO conditions: 10 °C min^{-1} in 5% O_2/He.

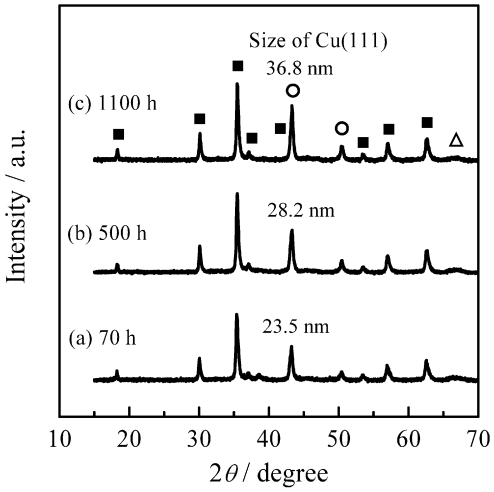

Fig. 8. XRD patterns of composite catalysts of $CuFe_2O_4$ and Al_2O_3 after reaction time-on-stream of (a) 70 h, (b) 500 h, and (c) 1100 h. Reaction conditions: S/C = 2.5, temperature (setpoint temperature) = 380 °C. (○) Cu, (■) Fe_3O_4, (△) Al_2O_3.

for the reaction tests so as to maintain the DME conversion below 100%; as a result, fast deactivation was not observed, suggesting that copper oxidation was negligible. Raman spectroscopy and XPS analyses confirmed the absence of $Cu(OH)_x$ in degraded catalysts. Postreduction of degraded catalysts in H_2 up to 350 °C did not lead to recovery of catalytic activity, indicating that copper oxidation was not dominant in the deactivation mechanism. In addition, no carbonate or formate groups were observed by Raman analysis, and the feed was free of poisonous species, such as sulfur and chloride; therefore, there was no catalyst poisoning on the catalyst. Accordingly, copper sintering and carbon deposition may be the main causes of deactivation.

The amount of carbon deposited on the catalyst was determined by temperature-programmed oxidation (TPO). Fig. 7 shows the desorption curves of CO_2 measured by mass spectrometry (MS) during TPO analysis of fresh, degraded, and regenerated composite catalysts. Large amount of CO_2 was released from the degraded catalyst during TPO, whereas peaks for CO_2 formation over the fresh and composite catalysts regenerated at 375, 500, and 700 °C were not evident in the TPO profiles. The carbon content in the degraded catalyst was determined as 0.124 mg g_{cat}^{-1}, whereas only trace amounts were detected in the fresh and regenerated catalysts. The TPO analysis indicated that carbon deposition was a cause of the deactivation. It is noteworthy that CO_2 was always observed on TPO analysis of degraded catalysts tested in various conditions, and that no CO_2 was detected after the calcination of the degraded catalysts in air for regeneration. Carbonaceous species deposited during DME SR can be removed even at a low temperature of 375 °C, suggesting that the formed carbon species were nongraphitic. Note that carbon monoxide was not detected during all of the TPO analyses.

XRD patterns of a composite catalyst as a function of reaction time are depicted in Fig. 8. Three crystalline phases of metallic Cu, Fe_3O_4, and γ-Al_2O_3 were detected in all of the XRD patterns. The crystallite size of copper determined by XRD-line broadening was obviously increased with increasing reaction. This result demonstrates that sintering of Cu proceeded during DME SR and was another factor contributing to deactivation. The concomitant effect of carbon deposition and Cu sintering can be considered the main reason for deactivation of the composite of $CuFe_2O_4$ and alumina. These findings indicate that lowering the reaction temperature or/and increasing the steam-to-carbon ratio can be effective in prolonging catalyst life.

3.4. Kinetics of reforming reaction and degradation

The reaction mechanisms of DME SR compose the elementary steps of DME hydrolysis and MeOH SR. Their kinetic parameters in DME SR have not been reported to date. The MeOH SR reaction over Cu-based catalysts is known to follow a pseudo-first-order reaction rate [25–27]. DME hydrolysis is confined by thermodynamic equilibrium, making it more complex. Although hydrolysis of DME to MeOH is limited by chemical equilibrium, the MeOH produced consecutively is reformed to hydrogen. Rapid conversion of the resultant MeOH shifts DME hydrolysis forward. Because MeOH was not detected during the reaction tests throughout the temperature range studied, DME SR reaction over the present catalysts is not limited by the chemical equilibrium of DME hydrolysis. Consequently, the kinetic parameters of DME SR were evaluated based on the following assumptions: (1) There is a pseudo-first-order reaction (excess steam at S/C = 2.5), (2) the reactor is an isobaric plug flow reactor, and (3) side reactions are neglected. The kinetic constant at a given temperature was then calculated from

$$k = -\frac{1}{\tau}\big[\varepsilon X + (1+\varepsilon)\ln(1-X)\big], \tag{6}$$

where k, τ, X, and ε are the reaction rate constant, the DME-based space time, the fractional conversion, and the theoretical

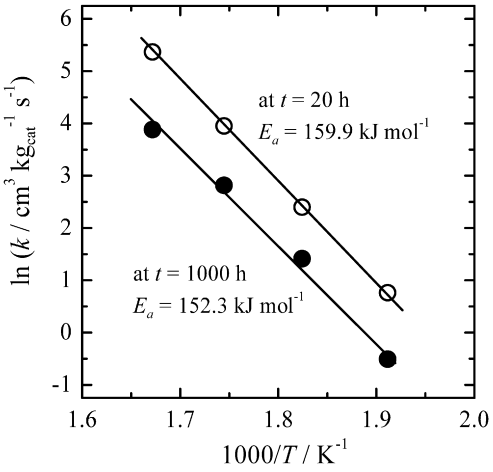

Fig. 9. Arrhenius plots for DME SR over composite of $CuFe_2O_4$ and Al_2O_3. Reaction conditions: as in Fig. 2.

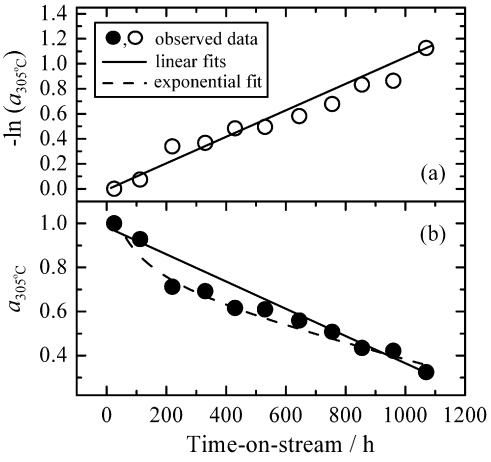

Fig. 10. Plots of power law deactivation model for DME SR over composite of $CuFe_2O_4$ and Al_2O_3: (a) first order and (b) zero order. Symbols and lines represent observed data at 305 °C and model fits, respectively. Reaction conditions: as in Fig. 2.

fractional expansion of the system based on DME, respectively. Plots of k values estimated from Eq. (6) at temperatures below 330 °C against temperature provide apparent activation energy and a preexponential parameter that can be estimated from Arrhenius equation [Eq. (7)],

$$k = A_0 \exp\left(-\frac{E_a}{RT}\right), \tag{7}$$

where k, E_a, A_o, R, and T are the reaction rate constant, the apparent activation energy, the preexponential factor, the gas constant, and the absolute temperature, respectively. Arrhenius plots in Fig. 9 at reaction times of 20 and 1000 h exhibited a good linearity. This indicates that the assumptions are acceptable. The apparent activation energy was calculated to be 159.9 and 152.3 kJ mol^{-1} at reaction times of 20 and 1000 h, respectively; no significant change of the activation energy was observed during the test, although partial degradation proceeded. This indicates that the dominant reaction mechanism over the catalyst remained unchanged, and that the chemical state of active species involved in DME SR was stable.

Deactivation kinetics of DME SR over spinel–alumina composite was studied by using power-law equation, which is a commonly used model for kinetic analysis of deactivation [28,29].

$$-r_d = -\frac{\mathrm{d}a}{\mathrm{d}t} = k_d a^d, \tag{8}$$

where r_d and k_d are the deactivation rate and the deactivation rate constant (h^{-1}), respectively, a is the relative activity of catalyst at time t (h), and d is the order of deactivation. This approach is based on the assumptions that concentration of active sites is a time-dependent power function of that of remaining active sites, and the deactivation rate is independent of chemical species taking part in the reactions. Integration of Eq. (8) when $d = 0$ and 1, with initial limits $t = 0$ and $a = 1$, gives the following equations:

$$a = 1 - k_d t, \quad \text{zero order } (d = 0) \tag{9}$$

and

$$-\ln(a) = k_d t, \quad \text{first order } (d = 1). \tag{10}$$

The relative activity was taken from the data at a representative temperature of 305 °C, where DME conversion was <100%. This is because this model for deactivation is not applicable to the temperature range in which the reaction rate is so high as to attain complete conversion, and thus it is hard to observe apparent activity change from the decrease in the conversion with reaction time. The relative activity was the ratio of reaction rate at time t (h) divided by that at 20 h to exclude the effect of phase change in the beginning of tests. The plots of the two equations are depicted in Fig. 10. The linearity of the plot of Eq. (9) is poor, whereas the plot agreed fairly well with the first-order deactivation kinetics with an exponential fit [Eq. (10)]. The deactivation rate constant was determined as 0.95×10^{-3} h^{-1}. It should be noted that a huge deviation of relative activity was found from the fit to second- and third-order deactivation kinetics (results not shown).

Alternatively, deactivation kinetics was evaluated based on the relationship between k and reaction time. The reaction rate constant k at 380 °C was calculated by using the Arrhenius equation. It was found that ln(k) was correlated well with reaction time as shown in Fig. 11. The linearity of the fit was fairly good, except for the beginning of the test. The good linearity of ln(k) with reaction time after ca. 100 h suggests that degradation proceeds in first-order kinetics, which is consistent with the kinetic analysis by the power law model expressed by Eq. (10). The degradation rate over the catalyst was expressed as follows:

$$\ln(k) = k_d t + c, \tag{11}$$

where k, k_d, t, and c are the reaction rate constant (cm^3 kg$_{cat}^{-1}$ s^{-1}), the degradation rate constant (h^{-1}), reaction time (h), and the constant, respectively. The deactivation rate constant was determined as 1.04×10^{-3} h^{-1}, which is in good agreement with that obtained using the direct approach of the

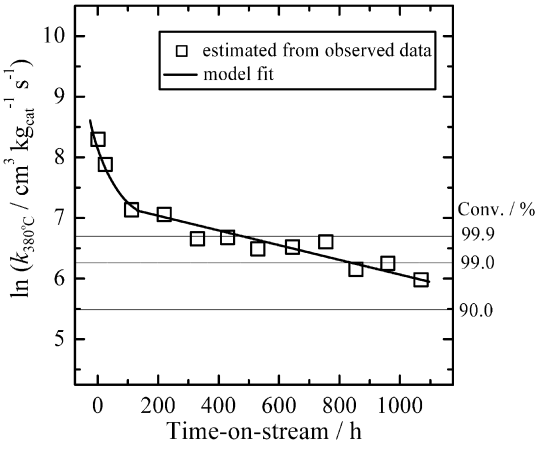

Fig. 11. Plot of ln(k) against time-on-stream for DME SR over composite of $CuFe_2O_4$ and Al_2O_3. Reaction conditions: as in Fig. 2.

power law model by Eq. (10). The resulting model would be a useful tool for predicting the catalyst lifetime.

4. Conclusions

Deactivation and regeneration behaviors of the composite catalysts of copper iron spinel and alumina in DME SR have been studied and concluding remarks were drawn as follows:

- On the long-term DME SR reaction test for 1100 h, the composite catalyst exhibited high durability with high rate for hydrogen production. Complete conversion of DME was maintained for 800 h under the reaction conditions of GHSV = 2000 h^{-1}, S/C = 2.5, and reaction temperature of 350–380 °C.
- Partial degradation of composite was due to the concomitant effects of copper sintering and carbon formation. Increasing steam-to-carbon ratio and/or decreasing reaction temperature would prolong the life of catalysts.
- The degraded catalyst was fully regenerated by calcination in air in the temperature range of 500–700 °C. Both redispersion of copper species through spinel reformation and carbon burning were achieved simultaneously, resulting in the recovery of catalytic performance.
- The apparent activation energy of DME SR over the composite remained stable at ca. 150–160 kJ mol^{-1} during the reaction test for 1100 h. The degradation kinetics was expressed well by a power law model and the logarithm of the DME SR reaction rate constant followed first-order deactivation kinetics with respect to reaction time.

Acknowledgments

This research was carried out as a joint research project, "Development of Hydrogen Production Catalysts Based on Spinel Oxides for Fuel Cell Application," by Kyoto University, Idemitsu Kosan Co., Ltd., and Japan Science and Technology Agency (JST) Innovation Plaza Kyoto.

References

[1] A.B. Stambouli, E. Traversa, Renew. Sust. Energ. Rev. 6 (2002) 295.
[2] T.A. Semelsberger, R.L. Borup, H.L. Greene, J. Power Sources 156 (2006) 497.
[3] H. Kobayashi, N. Takezawa, C. Minochi, J. Catal. 69 (1981) 487.
[4] P.H. Matter, D.J. Braden, U.S. Ozkan, J. Catal. 223 (2004) 340.
[5] E.S. Ranganathan, S.K. Bej, L.T. Thompson, Appl. Catal. A 289 (2005) 153.
[6] B.L. Kniep, F. Girgsdies, T. Ressler, J. Catal. 236 (2005) 34.
[7] T. Tanabe, S. Kameoka, A.P. Tsai, Catal. Today 111 (2006) 153.
[8] J. Papavasiliou, G. Avgouropoulos, T. Ioannides, Catal. Commun. 6 (2005) 497.
[9] V.V. Galvita, G.L. Semin, V.D. Belyaev, T.M. Yurieva, V.A. Sobyanin, Appl. Catal. A 216 (2001) 85.
[10] K. Takeishi, H. Suzuki, Appl. Catal. A 260 (2004) 111.
[11] Y. Tanaka, R. Kikuchi, T. Takeguchi, K. Eguchi, Appl. Catal. B 57 (2005) 211.
[12] T. Mathew, Y. Yamada, A. Ueda, H. Shioyama, T. Kobayashi, Appl. Catal. A 286 (2005) 11.
[13] T. Nishiguchi, K. Oka, T. Matsumoto, H. Kanai, K. Utani, S. Imamura, Appl. Catal. A 301 (2006) 66.
[14] K. Faungnawakij, Y. Tanaka, N. Shimoda, T. Fukunaga, S. Kawashima, R. Kikuchi, K. Eguchi, Appl. Catal. A 304 (2006) 40.
[15] T.A. Semelsberger, K.C. Ott, R.L. Borup, H.L. Greene, Appl. Catal. B 65 (2006) 291.
[16] T. Kawabata, H. Matsuoka, T. Shishido, D. Li, Y. Tian, T. Sano, K. Takehira, Appl. Catal. A 308 (2006) 82.
[17] M. Nilsson, L.J. Pettersson, B. Lindstrom, Energy Fuels 20 (2006) 2164.
[18] K. Faungnawakij, Y. Tanaka, N. Shimoda, T. Fukunaga, R. Kikuchi, K. Eguchi, Appl. Catal. B 74 (2007) 144.
[19] K. Faungnawakij, R. Kikuchi, T. Matsui, T. Fukunaga, K. Eguchi, Appl. Catal. A 333 (2007) 114.
[20] S. Kameoka, T. Tanabe, A.P. Tsai, Catal. Lett. 100 (2005) 89.
[21] Y. Choi, S.G. Stenger, Appl. Catal. B 38 (2002) 259.
[22] A. Szizybalski, F. Girgsdies, A. Rabis, Y. Wang, M. Niederberger, T. Ressler, J. Catal. (2005) 297.
[23] S. Natesakhawat, R.B. Watson, X. Wang, U.S. Ozkan, J. Catal. 234 (2005) 496.
[24] N. Laosiripojana, S. Assabumrungrat, Appl. Catal. B (2005) 107.
[25] H. Purnama, T. Ressler, R.E. Jentoft, H. Soerijanto, R. Schlögl, R. Schomäcker, Appl. Catal. A 259 (2004) 83.
[26] Y. Choi, H.G. Stenger, J. Power Sources 142 (2005) 81.
[27] B. Frank, F.C. Jentoft, H. Soerijanto, J. Kröhnert, R. Schlögl, R. Schomäcker, J. Catal. 246 (2007) 177.
[28] O. Levenspiel, Chem. Eng. Sci. 25 (1980) 1821.
[29] X. Huang, N.W. Cant, M.S. Wainwright, L. Ma, Chem. Eng. Process. 44 (2005) 403.